applied sciences

MDPI

Article

Parametric and Statistical Study of the Wing Geometry of 75 Species of Odonata

Nasim Chitsaz [1,*], Romeo Marian [1], Amirmasoud Chitsaz [2] and Javaan S. Chahl [1,3]

[1] School of Engineering, University of South Australia, Adelaide, SA 5095, Australia; romeo.marian@unisa.edu.au (R.M.); Javaan.Chahl@unisa.edu.au (J.S.C.)

[2] Faculty of Computer Engineering, Najafabad Branch, Azad University, Najafabad 8514143131, Iran; am_chitsaz@sco.iaun.ac.ir

[3] Joint and Operations Analysis Division, Defence Science and Technology Group, Edinburgh, SA 5111, Australia

* Correspondence: nasim.chitsaz@mymail.unisa.edu.au

Received: 18 June 2020; Accepted: 28 July 2020; Published: 4 August 2020

check for updates

Abstract: The flight performance and maneuverability of Odonata depends on wing shape and aero-structural characteristics, including airfoil shape, wingspan, and chord. Despite the superficial similarity between Odonata planforms, the frequency with which they are portrayed artistically, and the research interest in their aerodynamics, those features that are stable and those that are labile between species have not been identified. Studies have been done on 2D aerodynamics over corrugated wings; however, there is limited comparative quantified data on the planforms of Odonata wings. This study was undertaken to explore the scale relationships between the geometrical parameters of photogrammetrically reconstructed wings of 75 Odonata species, 66 from *Epiprocta*, and 9 from *Zygoptera*. The wing semi-spans captured in the database range from 24 to 85 mm. By carrying out an extensive statistical analysis of data, we show that the geometrical parameters for the suborder *Epiprocta* (dragonflies) can be classified into scale-dependent and independent parameters using regression analysis. A number of close correlations were found between the wingspan and the size of other structures. We found that amongst the variables considered, the largest independent variations against the forewing span were found in the chord of the hindwing, and that hindwing properties were not reliably predicted by the Odonata family. We suggest that this indicates continuous evolutionary pressure on this structure.

Keywords: aerodynamics; dragonfly; micro air vehicle (MAV); Odonata; 3D reconstruction

---

1. Introduction

There are various structural and aerodynamic demands related to the ecological niche of each species of Odonata that have influenced the characteristics of their wings through natural selection. An understanding of the aerodynamic performance of wings may inform considerations of metabolism, ecology, and evolutionary processes. Unlike many insects, Odonata wings have comparatively high aspect ratios [1], modest wing beat frequencies (30–40 Hz) [2–4], limited stroke angles (30°–60°) [5,6], and are used in gliding flight modes [7]. Some steady-state aerodynamic parameters are worth considering under these circumstances [8,9].

Odonata are categorized into the suborders *Epiprocta* (dragonflies) and *Zygoptera* (damselflies) [10]. The nodus size has been identified as an important parameter in the structure of a dragonfly wing, as illustrated in Figure 1b. The nodus is the point where the camber of the leading edge spar inverts [11], which is believed to provide strength and flexibility in flight [12]. Zhang et al. studied the dynamics of the nodus and wing in gliding flight [13]. According to their experimental visualization analysis, the nodus is an essential structural element of the wing, providing flexibility to the wing under aerodynamic loads [13]. The scanning electron microscopy (SEM) visualization and tensile testing have shown that the location of the nodus is critical during flight, due to high tensile stresses [14]. It also provides the wings with shock-absorbing capability that may help in dealing with any externally imposed torsion or bending stress [11]. During the flight, the wings undergo passive twist that is largely dependent on the position of the nodus [15]. The nodus is located at the leading edge at the interface of the second main vein and the leading edge of the wing where the orientation of the leading edge changes [16,17], which is about 50% of wingspan from the root [18,19]. The other prominent structure is the pterostigma. It is often found in the outer part of the span at the leading edge of Odonata wings, and is created by a blood-sinus during emergence [15] (Figure 1). Pterostigma probably plays a major role in the flight stability of Odonata. The concentrated mass of the pterostigma is believed to have a counteracting role during undesired twisting of the wing in the airflow [20]. As shown in Figure 1, the definition of chord lines for Odonata is different compared to commercial aircraft. For Odonata, chord lines are defined to have an angle α to the reference body line, where α is the angle between a perpendicular line to the reference body line and the perpendicular line to the chord. However, for aircraft, chord lines are defined parallel to a fuselage [21].

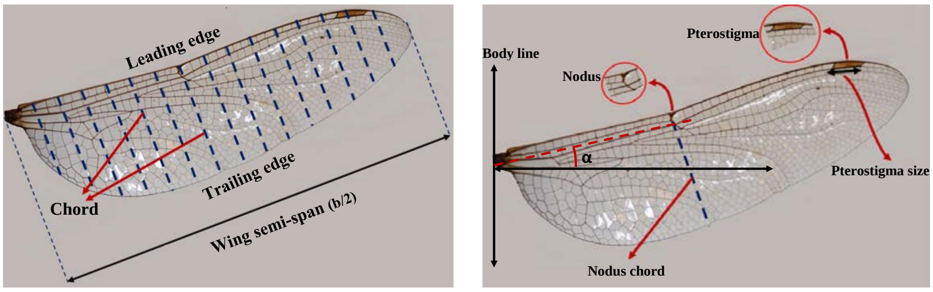

(a) (b)

Figure 1. Dragonfly wing geometry definition: geometrical parameters (**a**) and dragonfly wing geometry definitions nodus and pterostigma (**b**).

Odonata appear to have a characteristic arrangement of wings and overall planform common to all species, but with parameter variations. The purpose of our study was to explore how non-dimensional parameters might vary between species and scales of dragonflies for the next generation of the bio-inspired micro air vehicle. Our collection of 75 solid models of Odonata wings was measured to extract descriptive wing parameters. The main parameters of Odonata wings include forewing (FW) and hindwing (HW) span, minimum and maximum chord length, and location (these parameters play an important role to an optimum for the lift distribution over the wing) [22], nodus location and length, pterostigma size, and distance from the nodus. These parameters together describe the key features of an Odonata wing that are relevant to flight performance. Span and chord measurements have a significant role [23] in establishing the basic performance characteristics of fixed-wing aircraft, and are likely to be equally important to understanding the aerodynamic performance of Odonata. This paper presents the essential geometrical parameters of Odonata wings and explores the trends apparent in the dataset. The database and analysis procedure may be suitable for studies of ecology and evolution, as well as for advancing the design of small technological aircraft.

2. Materials and Methods

For this study, 75 wing geometries of various Odonata were captured from the collection of the South Australia Museum. Figure 2 shows the number of species of each family of Odonata species in the dataset. As shown in Figure 2, 50% are from the *Libellulidae* and *Aeshnidae* families that contain a large number of species with a wide range of sizes [24,25]. The 75 Odonata families and species are included from the *Libellulidae* family (*Libellula Pulchella, Libellula Murica Drury,* *Libellula Indica, Libellula Saturata, Lyriothemis Meyeri, Nesoxenia Mysis, Neurothemis Stig Matizans Bramina, Neurothemis Oligoneura, Orthetrum Caledonicum, Orthetrum Glaucum, Orthetrum Villosovittatum, Pantala Flave Scens, Lathrecista Asiatica, Protorthemis Coronata, Plathemis Lydia, Rhodothernis, Phyothemis Graphipters, Phyothemis Phyllis, Phyothemis Princeps, Tholymis Tillarga, Tramea Loewii, Zyxomma Sp, Huonia Thalassophila, Crocothemis Nigrifrons, Diplacina Phoebe, Camacinia Othello, Agrionopters Longitudinalis, Agrionoptera Insignis, Celithemis Eponina), Aeshnidae* family *(Adversaechna, Anax Guttatus, Anax Junius, Austroaeschna Multipunctata, Austroaeschna Parvistigma, Gynacantha Kirbyi, Gynacantha Mocsaryi, Dendroaeschna Conspersa, Hemianax, Notoaeschna Sagittata, Telephlebia Godeffroyi, Accessions), Corduliidae* family *(Epicordulia Princeps, Hemicordulia Australiae, Hemicordulia, Procordulia, Procordulia Jacksoniensis, Procordulia), Gomphidae* family *(Gomphus Crassus, Accessions, Dromogomphus Spoliatus, Hemigomphus Gouldii, Austrogomphus Prasinus, Ictinogomphus Australis), Calopterygidae* family *(Neurobasis Australis, Hetaerina Americana, Calopteryx Maculata, Playcypha, Papuagrion Occipitale*), *Macromiidae* family (*Macromia Tillyardi, Macromia Illinoiensis, Macromia Taeniolata*), *Petaluridae* family (*Petalura Ingentissima, Petalura Gigantea, Uropetala Carovei*), and *Synthemistidae* family (*Eusynthemis Brevistyla, Choristhemis Flavoterminate, Archaeosynthemis Orientalis*).

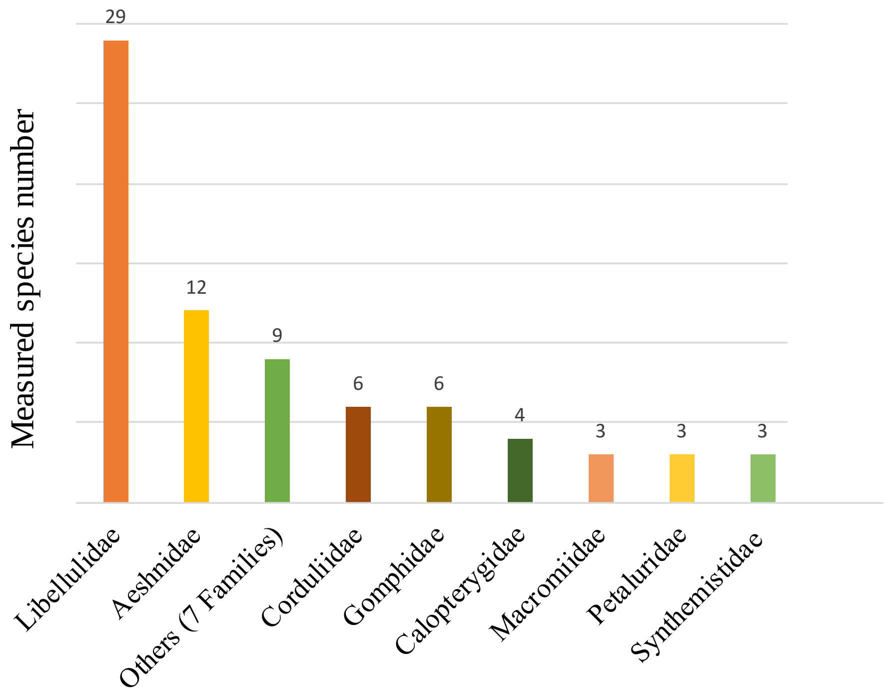

Figure 2. Number of each genus of Odonata, according to their species.

The dataset, including complete three-dimensional models, are available in the Dryad repository [26], with the original photographs from which the models were constructed. 3DF Zephyr Pro for photogrammetry and SolidWorks software for conversion of the point cloud to a solid model were used to reconstruct the wings [26,27]. Figure 3 shows the 3D reconstructed hindwing of a *Petalura Ingentissima* from the dataset. The dimensions of the wing and geometrical parameters were measured for both FW and HW from the projected files.

All specimens were from a publicly available Odonata collection in the South Australian Museum. Unfortunately, the entire collection has been classified by species, but has not been classified by sex. Furthermore, the collection specimens could not be accessed ventrally to establish their sex. The labeling of typical specimens is shown in the Appendix A. This is unquestionably a significant problem for some possible uses of this dataset, given the important role that sex might play in behavior, and thus functional demands on the flight apparatus. Considering further the implications of this limitation, we have studied many species with few individuals per species. We have considered wing shape, not the remainder of the anatomy. There are known sex-specific features in Odonata [28], albeit more subtle than in some species, such as butterflies [29,30]. Sex in dragonflies is established from ventral thoracic structures [31] rather than wing features. However, examining the spread of the data, there are no superficial indications of a bimodal distribution. This could only be expected if male and female Odonata had systematic differences that were large compared to variations between species. One implicit assumption in our study that results from this limitation is that the variations of non-dimensional parameters between species are greater than the variations between sexes.

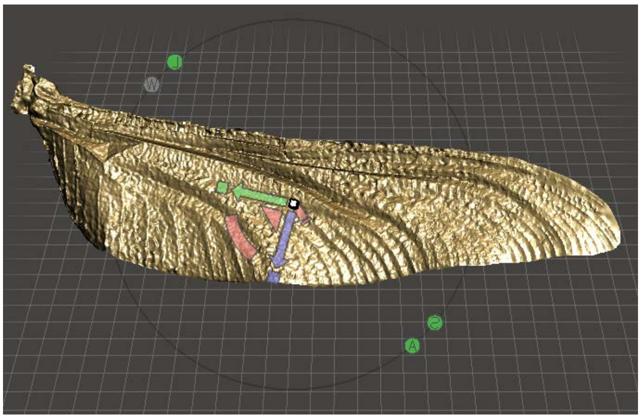

Figure 3. Three dimensional reconstructed of a *Petalura Ingentissima* hindwing.

The precision of the reconstruction of the wings in both surface dimensions and depth of angles/corrugation patterns was evaluated against a measured transparent flat model wing and Micro-CT, respectively, with good agreement between results (Figure 4). The method and validation are documented in Chitsaz et al. [26].

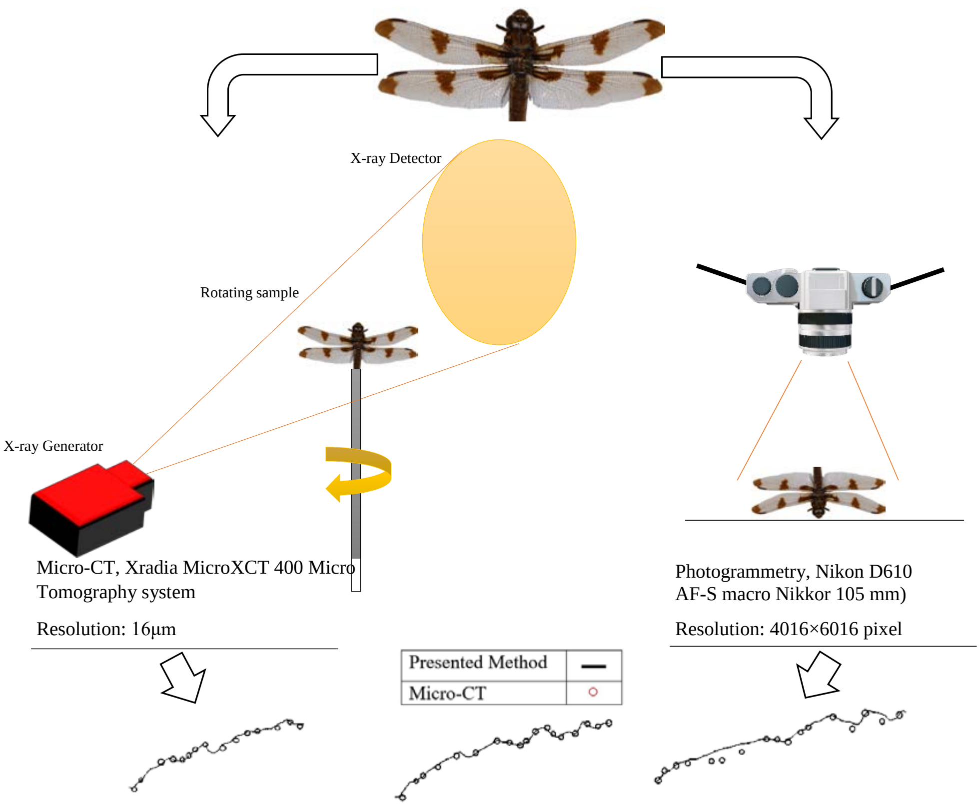

Figure 4. Schematic view of photogrammetry and Micro-CT process.

Wing Geometry and Parameter Definition

In this section, the measured wing geometry parameters are presented. We have defined wing geometry to be consistent with standard aeronautical definitions where possible [32,33]. However, due to the additional features of Odonata wings compared to aircraft and the tandem configuration [34], there are some additional definitions presented for the nodus and pterostigma. Figure 1 shows a schematic of dragonfly wing geometry and defined parameters [35]. The definition of the chord is the same as in aeronautics; chord refers to the imaginary straight line joining the leading edge (LE) and trailing edge (TE) of an airfoil that comes from the projected area of the reconstructed 3D wings and is perpendicular to the span. $b/2$ is wing semi-span (half wingtip-to-wingtip span). Maximum chord (C_{max}) is the longest straight line from wing LE to TE [9,36].

The other defining feature of the wing is the pterostigma (pigmented area), which is located close to the LE, which has a higher density than the rest of the wing [37]. This feature is also believed to be key to increasing critical speed in glide [20]. These eight parameters that describe the Odonata wings in our dataset are illustratively presented in the next section, and include wing semi-span, maximum chord, maximum chord location, mean chord, nodus chord, nodus chord location, pterostigma length, and location.

3. Results

The results include the geometrical parameters of wings from a total of 75 species from 15 families of Odonata that were measured from the projected area of the 3D digitized wings. The measured wing planform parameters include wing semi-span ($b/2$), maximum chord (C_{max}), location of the maximum chord ($C_{max,L}$), mean chord length of the wing (C_{mean}), nodus chord (C_{nodus}), which is the straight distance from LE to TE at the nodus, its location from the span coordinate of dragonfly body ($C_{nodus,L}$), length of pterostigma ($S_{pterostigma}$), and distance of nodus to pterostigma (D) for both FW and HW. All parameter dimensions are in millimeters.

3.1. Database Analysis

In order to get a better understanding of the range in the processed data, initial results are shown with the probability (area under the curve) and fitted normal distributions. Since it is possible that no subsequent large study will be undertaken of dragonfly species' wings, we have treated the sample as if it were randomly selected. In a collection, there is every likelihood that this is not the case for the most superficially obvious parameters, such as size, and other hidden indirect considerations leading to ease of capture of specimens. We assumed that derived measures and ratios were less likely to be biased by the process of sampling. Equation (1) shows the formula for calculating the probability of normal distribution.

$$f(x \mid \mu, \sigma^2) = \frac{1}{\sqrt{2\pi\sigma\hat{}2}} e^{-\frac{(x-\mu)2}{2\sigma 2}} \quad (1)$$

where μ, σ, and $\sigma\hat{}2$ are the mean, standard deviation, and variance, respectively, and x is the desired measured parameter [38].

Figure 5 shows the range of half-span of HW and FW across the collection, according to their families. In this study, the species with the smallest wingspan was *Huonia thalassophila*, with dimensions of 47.32 and 46.50 mm. The largest wingspan was 168.84 and 169.54 mm, of *Petalura ingentissima (PI)*, the giant *petaltail* [39].

The maximum chord length was 16.24 mm and 20.92 mm for FW and HW, respectively. As shown in Figure 5, it is evident that the wingspan length of the Odonata wings can vary from 47 mm to 169 mm. Thus, in order to find a proper trend between the geometrical parameters of the wings, all of the studied parameters of each wing were non-dimensionalized with the semi-span length ($b/2$) of that wing. This is a useful approach to design an applicable micro air vehicle (MAV), in both aerodynamics and flight performance aspects, which is similar to general airplanes. Figure 6 shows the non-dimensional maximum chord and its location and non-dimensional mean chord normal distribution and probability density function (PDF) for both FW and HW. Results show that the average mean and maximum chord length of the HW is around 25% larger than corresponding measurements from the FW. The average value for Cmax/Cmean parameter is 1.4 for both HW and HW. The location of Cmax is also an interesting parameter in the overall shape of the wing. $C_{max,L}$ is the deterministic parameter for spanwise lift and drag distribution across the wing. Results show that $C_{max,L}/b$ has high scatter, with standard deviation of around 0.1.

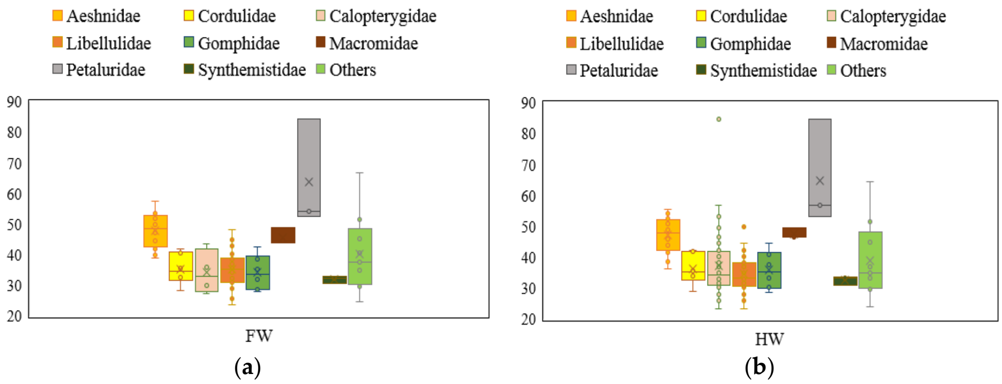

Figure 5. Semi-span distribution for both FW (**a**) and HW (**b**).

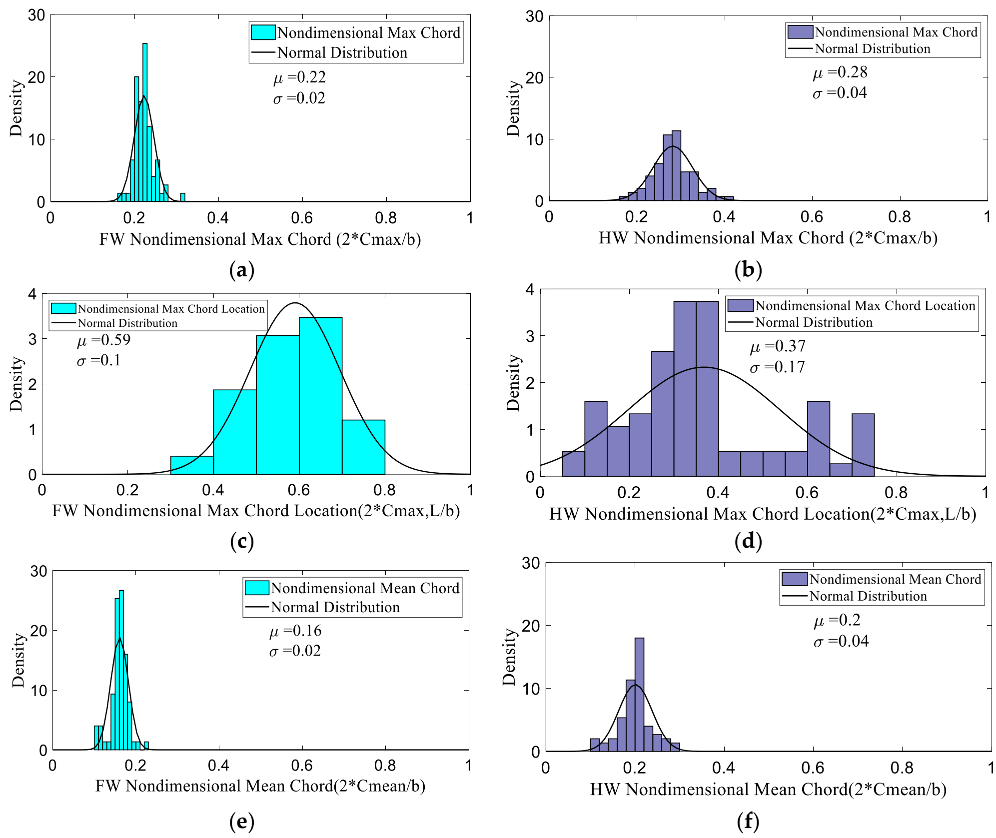

Figure 6. Probability density function (PDF) and fitted normal distribution of forewing (FW) max chord (**a**), hindwing (HW) max chord (**b**), FW max chord location (**c**), HW max chord location (**d**), and FW mean chord (**e**) and FW mean chord (**f**).

The PDF and normal distribution of nodus and pterostigma parameters from the sample, which are believed to be functional features of Odonata wings [20], were calculated. Figure 7 shows the non-dimensional normal distribution of nodus chord length, pterostigma size, and their locations for FW and HW. As shown below, the ratio of nodus to pterostigma location is 1.7 and 1.9 for FW and HW. The results show that the size of the pterostigma has a relatively high scatter. *Calopterygidae* and *Chlorocyphidae* do not have pterostigma. Also, it is found that for *Petalura Ingentissima*, 2 × pterostigma, $_{L}$/b is between 0.6–0.7.

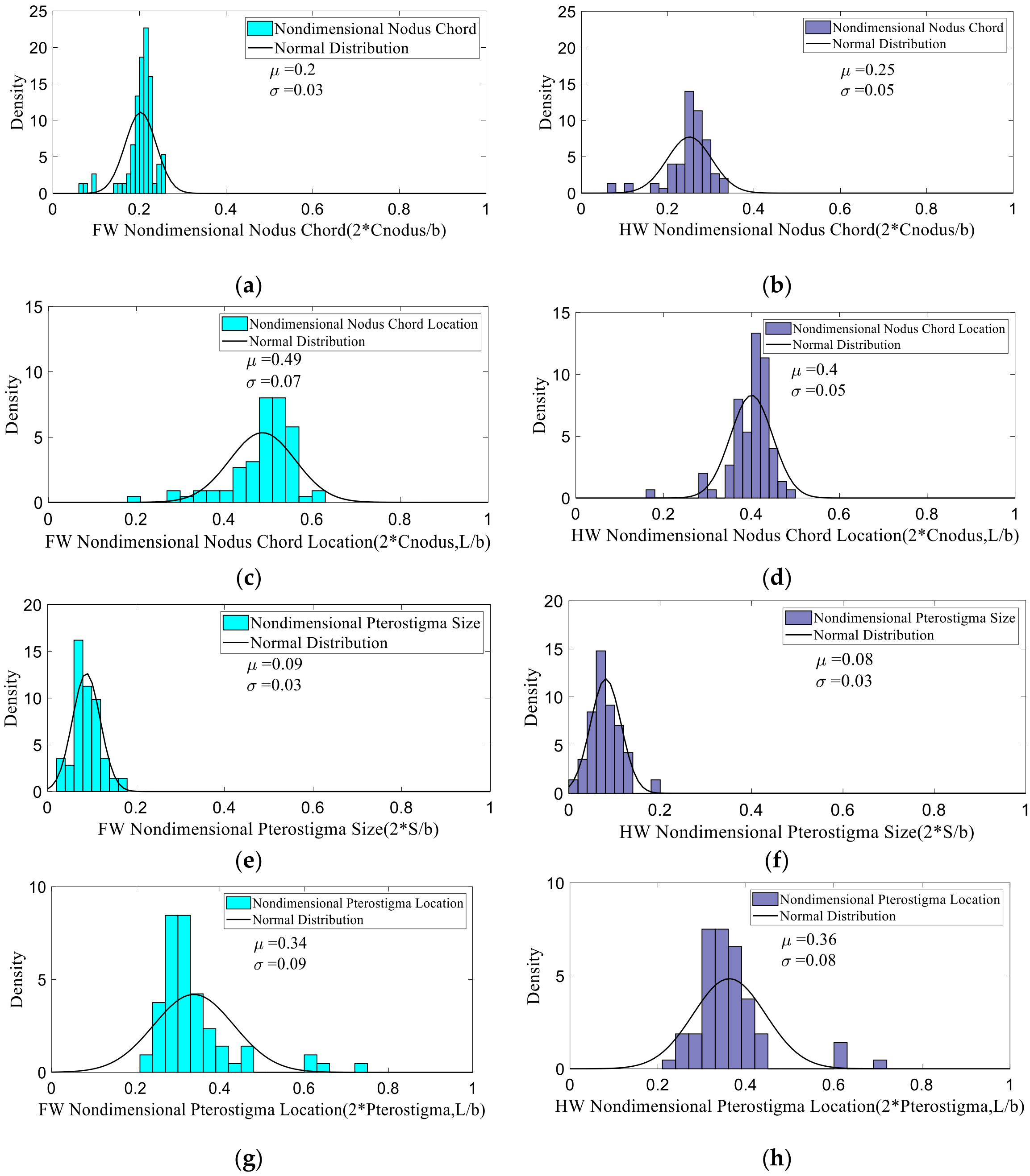

Figure 7. PDF and fitted normal distribution of FW nodus chord (**a**), HW nodus chord (**b**), FW nodus chord location (**c**), HW nodus chord location (**d**), FW pterostigma size (**e**), HW pterostigma size (**f**), FW pterostigma location (**g**) and HW pterostigma location (**h**).

The non-dimensional normal distribution of max chord, max chord location, mean chord nodus chord, nodus chord location, pterostigma size, and pterostigma location for both FW and HW for the same species of two families of *Aeshnidae* and *Libellulidae* are illustrated in Figures 8 and 9. These two figures were plotted to compare two families of *Aeshnidae* and *Libellulidae*, as they are nearly

50% of the dataset, and tend to be larger. By comparing two families, it is found that some parameters are dependent, such as $C_{max,L}$, and some are non-dependant, such as C_{max}. Also, for HW, the standard deviation differs between *Aeshnidae* and *Libellulidae*, compared with FW.

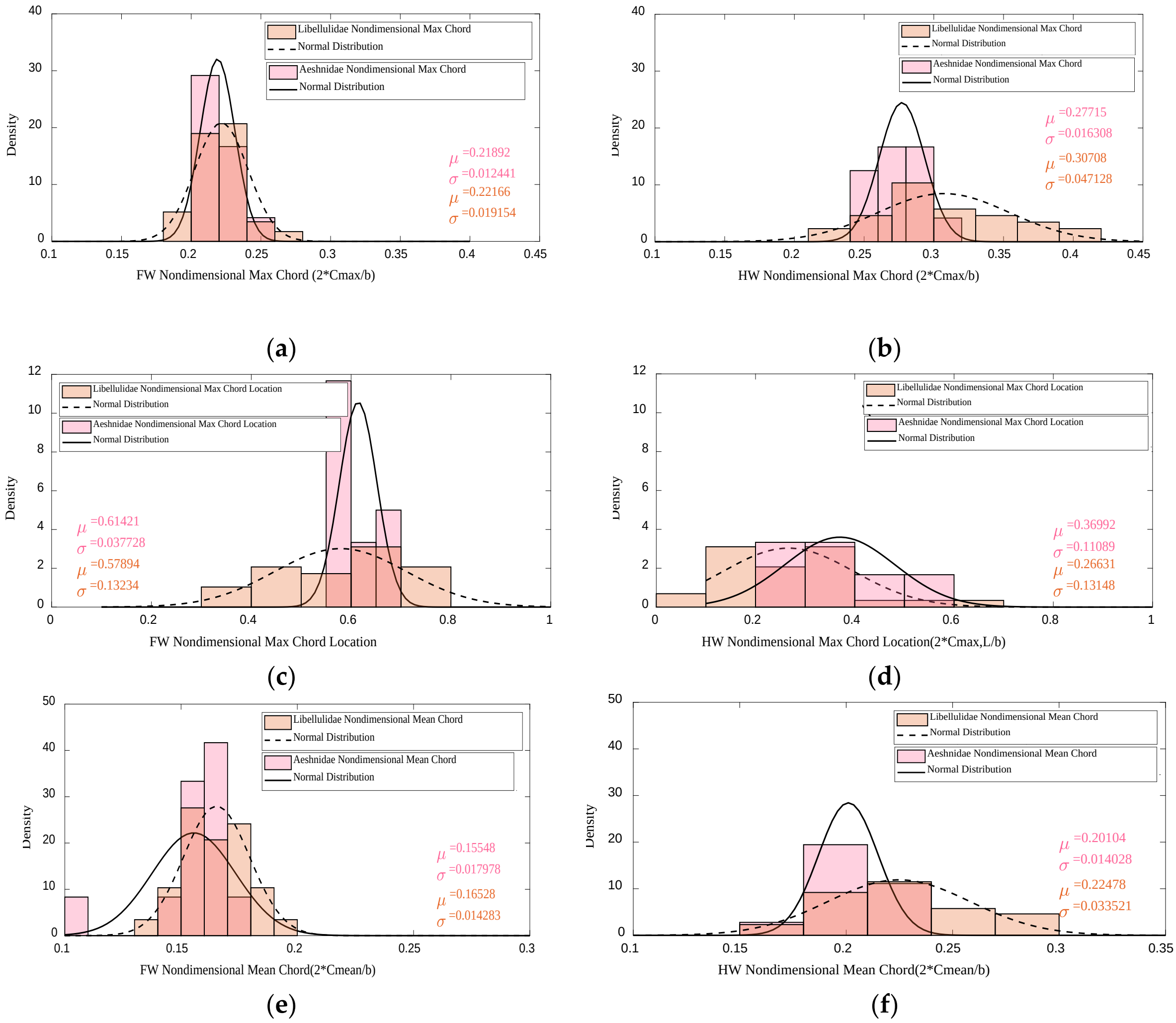

Figure 8. Probability density function and fitted normal distribution of non-dimensional parameters: FW max chord (**a**), HW max chord (**b**), FW max chord location (**c**), HW max chord location (**d**), HW mean chord (**e**) and HW mean chord (**f**) of the two families of *Aeshnidae* and *Libellulidae*.

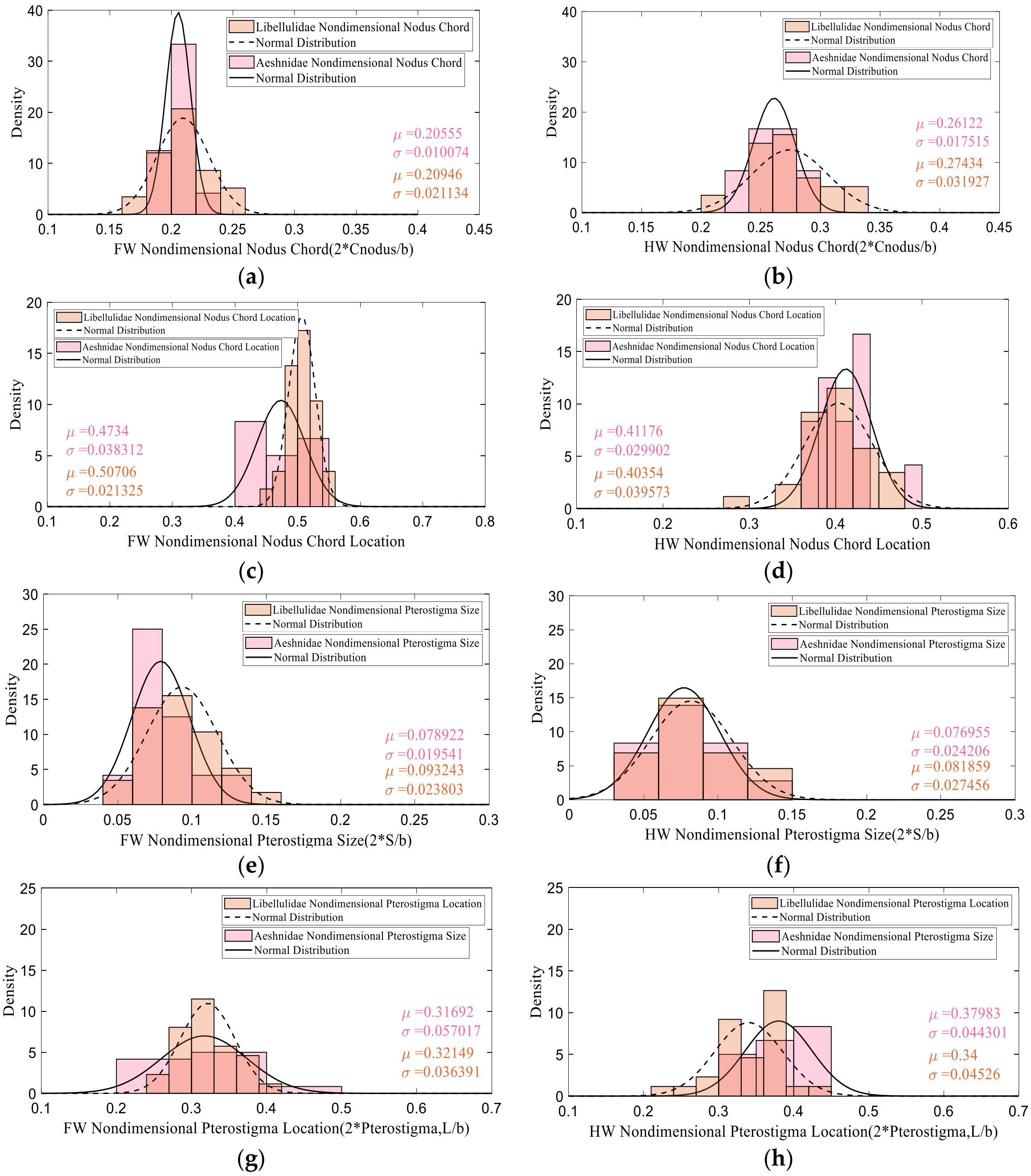

Figure 9. Probability density function and fitted normal distribution of non-dimensional parameters: FW nodus chord (**a**), HW nodus chord (**b**), FW nodus chord location (**c**), HW nodus chord location (**d**), FW pterostigma size (**e**), HW pterostigma size (**f**), FW pterostigma location (**g**) and HW pterostigma location (**h**) for both FW and HW of two families of *Aeshnidae* and *Libellulidae*.

3.2. Regression Analysis

The species studied included small species with a span length of 46 mm up to large ones with a span length of 170 mm. In this section, both linear and polynomial regression is presented for the seven measured parameters, including $b/2$, C_{max}, C_{mean}, C_{nodus}, $C_{nodus,L}$, pterostigma size, and location. A p-value of less than 0.05 is the criteria for accepting the regression equation [40]. Note that the objective of this section is to identify trends, particularly with respect to scale.

Figure 10 shows the wing semi-span ($b/2$) length versus the maximum chord of the FW with the minimum and maximum lengths of 5 mm and 16 mm, respectively. Both polynomial (y_1) and linear (y_2) regressions were found to be a satisfactory fit to find the C_{max} vs. $b/2$ for both FW and HW. In the following figures, the red dots correspond to *Zygoptera* (damselfly) order, while the black dots relate to *Epiprocta* (dragonfly) order, and both are suborders of Odonata. *Petalura Ingentissima* is a large dragonfly, but is a single sample very far from the other dragonflies in scale, so we have excluded it and the *Zygoptera* from regression fitting in the following.

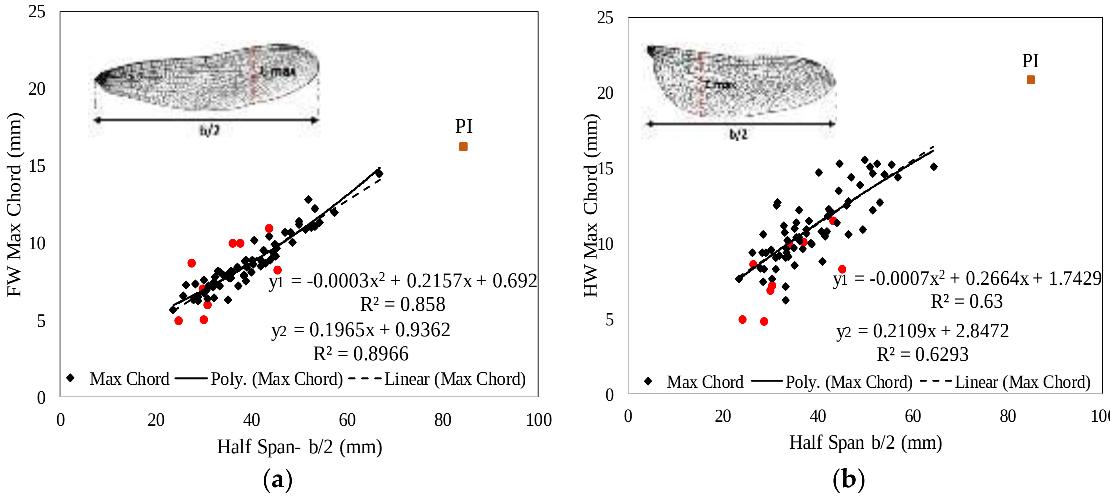

Figure 10. Maximum chord versus wing semi-span of the forewings (**a**) of dragonflies, and maximum chord versus wing semi-span of the hindwings (**b**) of dragonflies.

Figure 11 illustrates wingspan versus the mean chord of FW and HW, respectively. Similarly, both polynomial (y_1) and linear (y_2) regressions predict the relationship between the mean chord and the half-span for both FW and HW.

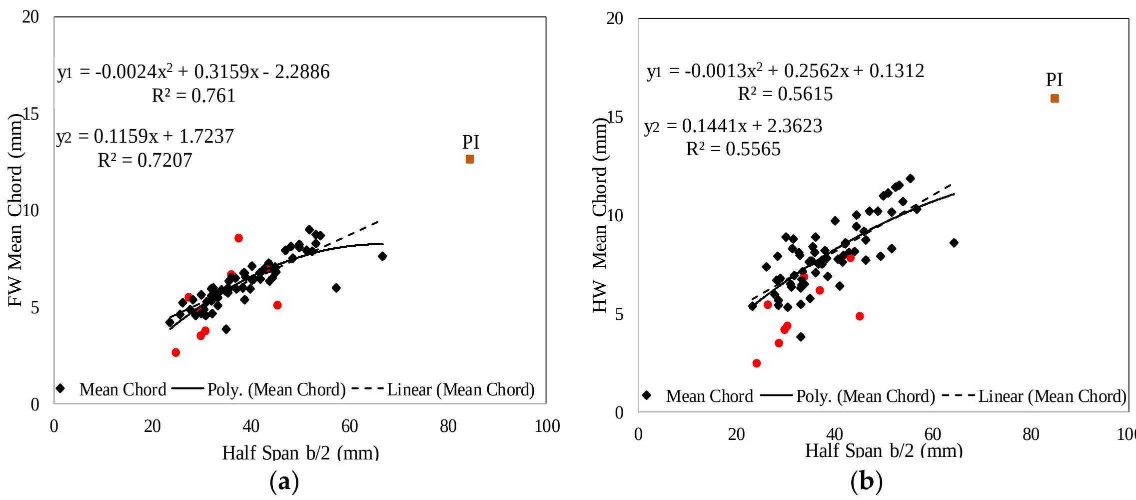

Figure 11. Mean chord versus wingspan of the forewings (**a**) of dragonflies, and mean chord versus wingspan of the hindwings (**b**) of dragonflies.

It has previously been proposed that the nodus plays an essential role in wing structural flexibility, which has led to a nodus structured wing being used in an MAV [19]. The definition of the nodus chord (C_{nodus}) for FW and HW is demonstrated in Figure 12.

The position and size of the pterostigma are believed to be important in dynamically regulating wing pitch angle by harnessing inertial forces [20]. Figure 13a,b graphs $b/2$ versus nodus chord location and pterostigma location (Lpterostigma) of FW and HW, respectively, with polynomial and linear trends for the distribution. It is apparent that the FW nodus location to mid-span is almost similar compared to the HW. However, 90% of both FW and HW nodus are concentrated between 20% and 60% of wing semi-span. Strong correlation is found between wingspan and pterostigma size for both FW and HW in Figure 13c. The red and green dots are related to *Zygoptera* family for FW and HW, respectively.

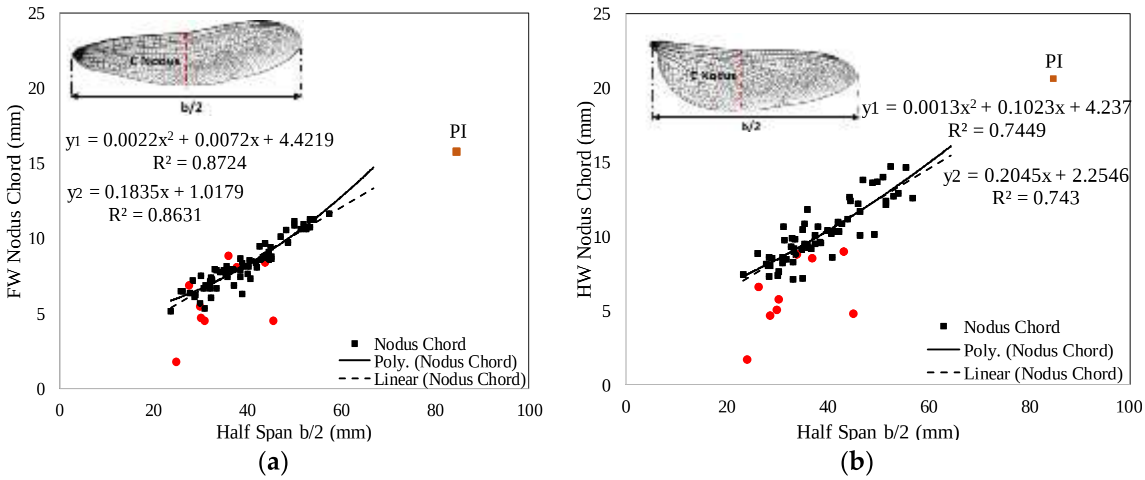

Figure 12. Nodus chord versus wing semi-span of forewings (**a**), and nodus chord versus wing semi-span of hindwings (**b**).

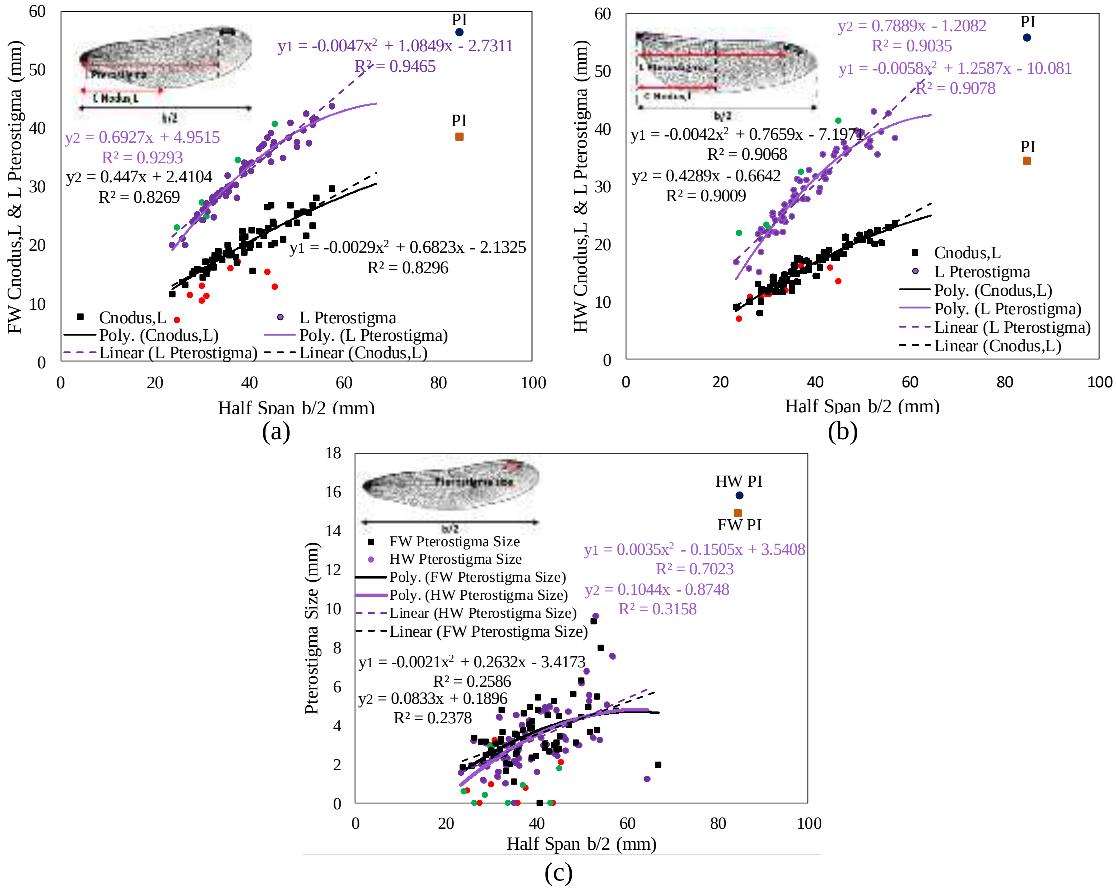

Figure 13. (**a**) Nodus chord and pterostigma location versus wing semi-span of the forewing, (**b**) nodus chord and pterostigma location versus wing semi-span of the hindwing, and (**c**) pterostigma size versus wing semi-span of the forewings and hindwings.

To better understand the correlation between the nodus and pterostigma, the nodus chord, nodus location, and pterostigma size and its location were normalized to wing semi-span. In the following, the non-dimensional parameters of nodus chord vs. pterostigma location (Figure 14a,b), nodus chord location vs. pterostigma location (Figure 14c,d), and pterostigma location vs. size (Figure 14e,f) for FW and HW are presented (Figure 14). The graph shows that nodus and pterostigma of FW and HW are still well-correlated for both families. Correlation is found for chord nodus vs. pterostigma for *Epiprocta*, being 40% to 60% of nodus chord, while for *Zygoptera*, it varies (Figure 14a,b).

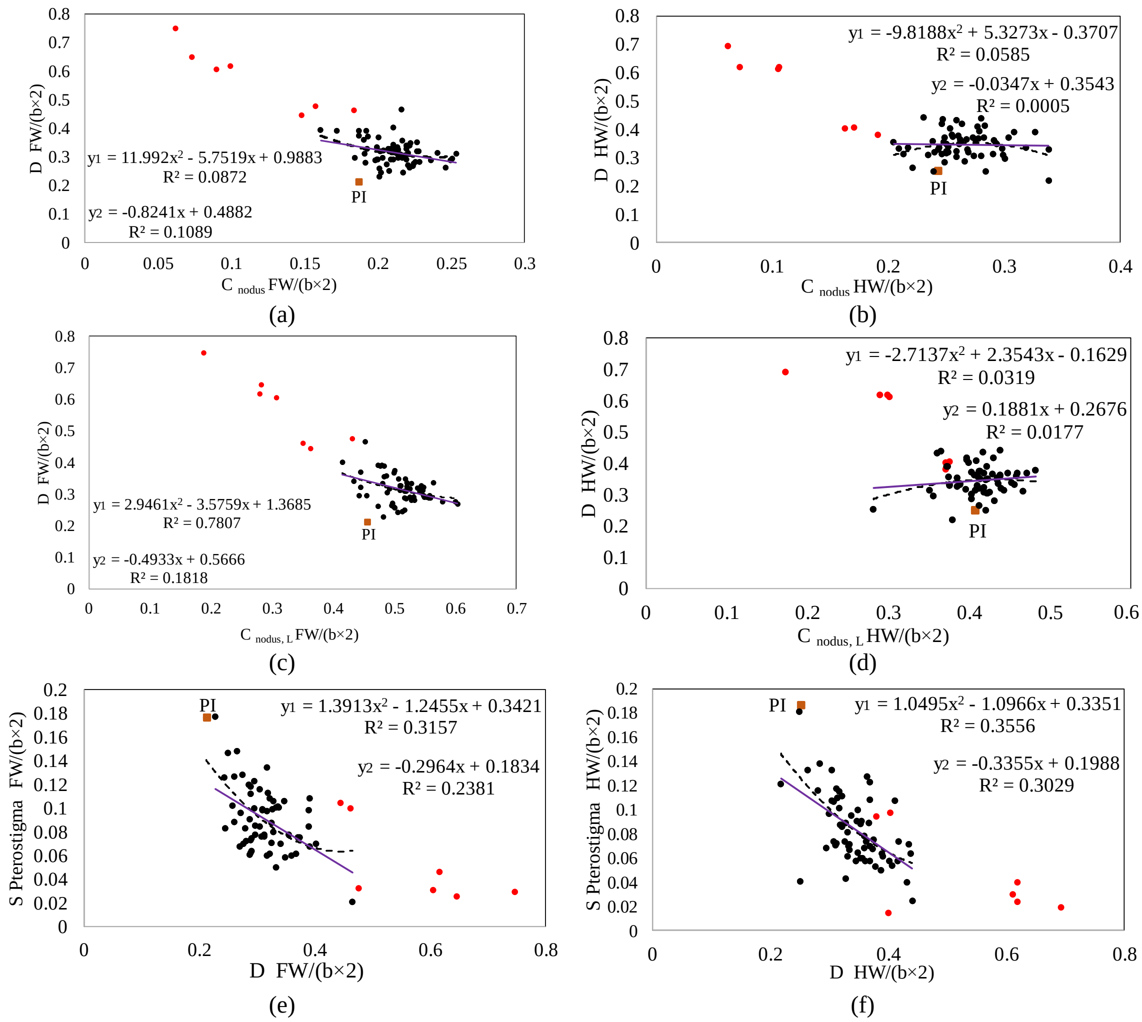

Figure 14. Nodus chord and pterostigma location versus wing semi-span of the forewings (**a**) and hindwings (**b**), nodus chord location and pterostigma location versus wing semi-span of the forewings (**c**) hindwings (**d**), and pterostigma size versus wing semi-span of the forewings (**e**) and hindwings (**f**).

3.3. Design Approach

Table 1 presents the essential parameters extracted from regression for all studied Odonata wings, including damselflies and dragonflies. Normalizing against wingspan makes it possible to export the other parameters of the wing and compare wing shape characteristics, despite scale variations. For instance, it has been shown that the pterostigma is located at 81% of the FW and 76% of HW.

Table 1. Essential wing geometrical parameters exported from the graphs.

Wing Geometry Parameter	R^2
C_{max} FW = 0.219 × (b/2)	0.86
C_{max} HW = 0.276 × (b/2)	0.70
$C_{max,L}$ FW = 0.58 × (b/2)	0.62
$C_{max,L}$ HW = 0.37 × (b/2)	0.27
C_{mean} FW = 0.16 × (b/2)	0.73
C_{mean} HW = 0.20 × (b/2)	0.63
b FW/HW = 1	-
$C_{nodus,L}$ FW = 0.489 × (b/2)	0.78
$C_{nodus,L}$ HW = 0.404 × (b/2)	0.91
$C_{pterostigma,L}$ FW = 0.811 × (b/2)	0.95
$C_{pterostigma,L}$ HW = 0.756 × (b/2)	0.91

These parameters were derived from our sample of specimens of many species and are independent of wing size. There is consistency and low deviation from the trend for some geometrical parameters, like the maximum chord for the whole species, which means that these parameters are independent of wing size and species. On the other hand, having a large deviation shows that the actual parameters for a species (Figures 8 and 9) are driven by other factors. Table 2 lists the nondependent and dependent variable parameters. For this case, it is assumed that the compiled results with R-squared correlation value of less than 0.7 are dependent parameters.

Table 2. List of family-dependent and nondependent geometric parameters of the dragonfly wing.

Nondependent Parameters ($R^2 > 0.7$)	Dependent Parameters ($R^2 < 0.7$)
C_{max}	$C_{max,L}$
C_{mean} FW	Pterostigma size
C_{nodus}	C_{mean} HW
$C_{nodus,L}$	-
$L_{pterostigma}$	-

The non-dimensional maximum, average, and minimum ratio of the dimension and location of the maximum chord, and also the nodus chord, for FW and HW are described in Table 3.

Table 3. Maximum, minimum, and average ratio for FW and HW.

	Forewing			Hindwing		
	Min.	Ave.	Max.	Min.	Ave.	Max.
$2 \times C_{max}/b$	0.17	0.22	0.32	0.17	0.27	0.40
$2 \times C_{max\ L}/b$	0.33	0.59	0.79	0.10	0.37	0.74
$2 \times C_{mean}/b$	0.10	0.16	0.23	0.10	0.20	0.30
$2 \times C_{nodus}/b$	0.06	0.20	0.25	0.06	0.247	0.34
AR	8.74	12.68	19.30	6.77	10.37	19.20

4. Discussion

Comparing average results, one can say that the dimension of the maximum chord is around 25% of the wing semi-span in the species measured. However, its location is closer to the body for the HW, which is 37% of the wing semi-span. Furthermore, the location of the maximum chord can be significantly different for different species. The minimum span location belongs to the HW of the *Libellulidae* family by a fraction of 0.1 of semi-span length. Among our dataset, the maximum chord is placed at approximately 79% of the FW semi-span. Figure 15 presents an illustrative example of the observed design criteria, regarding the minimum and maximum margins of the maximum chord and its location relative to the wing dimension (hatch-line areas). The hatch areas are the representative of the estimation range for both max chord and its location. In other words, the length of the hatch areas is representative of the range of the location of the max chord, which can vary from 0.33 to 0.8 of the semi-span length. On the other hand, the width of the hatch areas is representative of the max chord length, which can vary between 0.17 and 0.32 of the semi-span length.

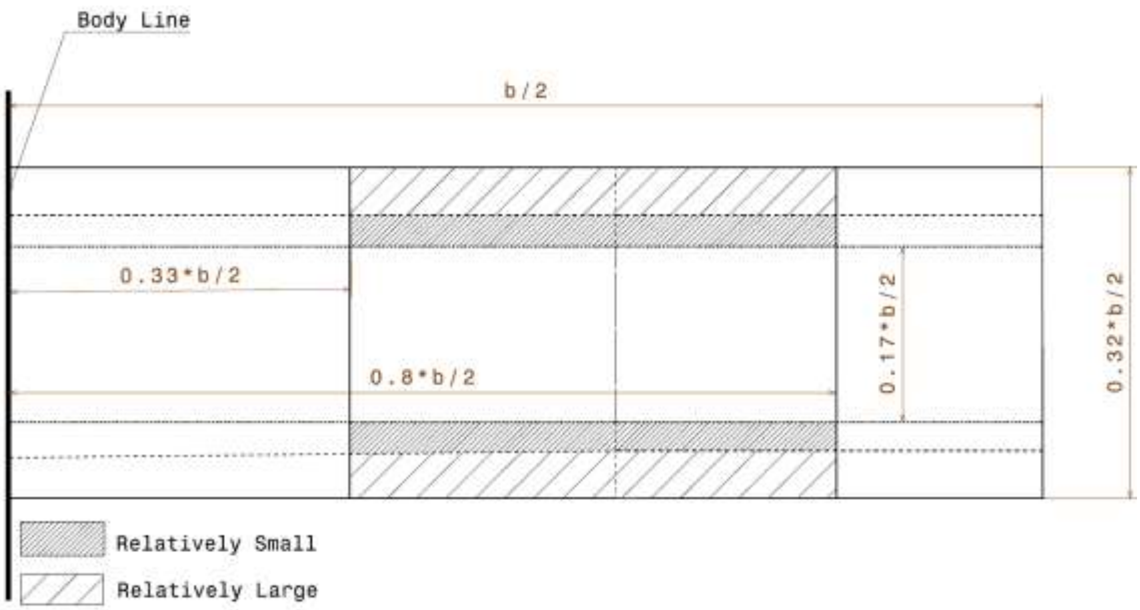

Figure 15. Non-dimensional estimation range of the FW max chord max, and its location through the wing semi-span.

This graph can be extended for the other parameters, such as pterostigma and nodus, to provide a general mapping algorithm for the preliminary design of a flapping wing drone aircraft. Another parameter shown in Table 3 is the aspect ratio (AR), which is generally defined as the ratio of full span to mean chord [41]. According to these data, the average AR is 12.68 and 10.37 for FW and HW, respectively. Pterostigma is the other significant factor for designing the bio-inspired wing. Possessing a favorable aerodynamic function, the pterostigma is located in close proximity to the tip of the wing as a dark, thickened membrane structure [14]. The pterostigma changes the center of mass of the wing at the leading edge, which leads to more stability in flapping flight [42]. The pterostigma is located near the wingtip; in *Aeshna Juncea* (one the large species of hawker dragonflies from the *Aeshnidae* family) they have mass relative to the FW and HW of around 9% and 16% respectively [43]. By comparing the results, it can be understood that the location of the pterostigma of the FW to HW ratio is 1.07. The size of the pterostigma appears to be weakly correlated with size and chord, which might be caused by evolution of flight performance and conspecific communication functions of the pterostigma both driving this feature.

Previous research has shown that the wings of damselfly and dragonfly are different [44]. This is also shown by our data, particularly relating to the nodus and pterostigma. In terms of overall dimensions and ratios of wing geometry, the *Zygoptera* and *Epiprocta* are statistically similar.

In the methods section, a limitation of the underlying collection of animals, and thus the study, was mentioned, which was that we could not determine the sex of the specimens. It seems reasonable to surmise that the variations by sex are less than variations between orders, and this study aimed to find the range of parameters and their trends against scale for the order Odonata.

The results regarding the placement of the nodus extend the data available in the literature [13], and reaffirm that the nodus is a significant structure.

Throughout the dataset, there is a trend of non-dimensional HW parameters having lower correlation against the trend and larger variation across the dataset than the FW, with species not being predictive of the variations. It may indicate that more recent adaptations, perhaps caused by variations in habitat or lifestyle, favor HW changes over FW changes.

5. Conclusions

In this study, a geometrical and basic planform study on the dragonfly wings from 75 samples of 15 different Odonata species families was performed. The diversity of species enabled us to document the geometry of the planform of the wings from the span length of 48 mm to 170 mm. The measured parameters were taken from the projected area of the 3D reconstructed models of the wings. The measurements were taken over the eight essential planform wing parameters for both FW and HW. These included wingspan length, mean and maximum chord length, maximum chord location, nodus location, pterostigma size, and location. An extensive statistical analysis of the data was performed to investigate the independence of the measured parameters from the families of the Odonata. In general, across the species studied, HWs appear to have the most variation in all dimensions measured compared to the FW, with family not being predictive of HW shape. Further work will try to identify functional reasons for scale-related variations. In addition, the shapes of Odonata wings are not similar, and this is an important parameter requiring further investigation in the future.

Author Contributions: Conceptualization: N.C., R.M., and J.S.C.; methodology: N.C. and J.S.C.; software: N.C., R.M., A.C., and J.S.C.; validation: N.C., A.C., and J.S.C.; formal analysis: N.C. and A.C.; investigation: N.C., A.C., and J.S.C.; resources: R.M. and J.S.C.; data curation: N.C., A.C., and J.S.C.; writing—original draft preparation: N.C.; writing—review and editing: N.C., R.M., A.C., and J.S.C.; visualization: N.C. and J.S.C.; supervision: R.M. and J.S.C.; project administration: N.C. and J.S.C.; funding acquisition: J.S.C. All authors have read and agreed to the published version of the manuscript.

Funding: This research received no external funding.

Acknowledgments: We would like to thank the South Australian Museum, Adelaide, for granting access to their collection of dragonflies used in this study. The first author is the recipient of the William T. Southcott Scholarship from the University of South Australia.

Conflicts of Interest: The authors declare no conflicts of interest.

Appendix A

Figure A1. Labeling of typical specimens at South Australian Museum.

References

1. Hassall, C. Strong geographical variation in wing aspect ratio of a damselfly, Calopteryx maculata (Odonata: Zygoptera). *PeerJ* **2015**, *3*, e1219. [CrossRef] [PubMed]
2. Saharon, D.; Luttges, M. Visualization of unsteady separated flow produced by mechanically driven dragonfly wing kinematics model. In Proceedings of the 26th Aerospace Sciences Meeting, Reno, NV, USA, 9–12 January 1989; p. 569.
3. San Ha, N.; Truong, Q.T.; Goo, N.S.; Park, H.C. Corrigendum: Relationship between wingbeat frequency and resonant frequency of the wing in insects (2013 Bioinspir. Biomim. 8 046008). *Bioinspir. Biomim.* **2015**, *10*, 019501.
4. Chen, J.-S.; Chen, J.-Y.; Chou, Y.-F. On the natural frequencies and mode shapes of dragonfly wings. *J. Sound Vib.* **2008**, *313*, 643–654. [CrossRef]
5. Rüppell, G.; Hilfert, D. The flight of the relict dragonfly Epiophlebia superstes (Selys) in comparison with that of the modern Odonata (Anisozygoptera: Epiophlebiidae). *Odonatologica* **1993**, *22*, 295–309.
6. Stanford, B.; Lacore, D.; Albertani, R.; Parker, G.; Walker, R.; Curtis, D. Proper Orthogonal Decomposition of Flexible Clap and Fling Motions via High-Speed Deformation Measurements. In Proceedings of the 48th AIAA Aerospace Sciences Meeting Including the New Horizons Forum and Aerospace Exposition, Orlando, FL, USA, 4–7 January 2010; p. 1026.
7. Bomphrey, R.J.; Nakata, T.; Henningsson, P.; Lin, H.-T. Flight of the dragonflies and damselflies. *Phil. Trans. R. Soc. B* **2016**, *371*, 20150389. [CrossRef]
8. Wakeling, J.; Ellington, C.P. Dragonfly flight. I. Gliding flight and steady-state aerodynamic forces. *J. Exp. Biol.* **1997**, *200*, 543–556.
9. Sun, X.; Gong, X.; Huang, D. A review on studies of the aerodynamics of different types of maneuvers in dragonflies. *Arch. Appl. Mech.* **2017**, *87*, 521–554. [CrossRef]
10. Brodsky, A.K. *The Evolution of Insect Flight*; Oxford University Press: Oxford, UK, 1994.
11. Wootton, R.J.; Newman, D.J. Evolution, diversification, and mechanics of dragonfly wings. In *Dragonflies and Damselflies: Model Organisms for Ecological and Evolutionary Research*; Oxford University Press: Oxford, UK, 2008; pp. 261–274.
12. Sun, J.; Bhushan, B. The structure and mechanical properties of dragonfly wings and their role on flyability. *Comptes Rendus Mécanique* **2012**, *340*, 3–17. [CrossRef]
13. Zhang, S.; Sunami, Y.; Hashimoto, H. Deformation behavior of dragonfly-inspired nodus structured wing in gliding flight through experimental visualization approach. *Sci. Rep.* **2018**, *8*, 5751. [CrossRef]
14. Rajabi, H.; Darvizeh, A. Experimental investigations of the functional morphology of dragonfly wings. *Chin. Phys. B* **2013**, *22*, 088702. [CrossRef]
15. Wootton, R.J. Functional morphology of insect wings. *Annu. Rev. Entomol.* **1992**, *37*, 113–140. [CrossRef]
16. Kesel, A.B. Aerodynamic characteristics of dragonfly wing sections compared with technical aerofoils. *J. Exp. Biol.* **2000**, *203*, 3125–3135. [PubMed]
17. Lindley, R. Some armchair thoughts on the dragonfly wing. *Odonatologica* **1978**, *7*, 323–351.
18. Chen, Y.; Skote, M.; Zhao, Y.; Huang, W. Dragonfly (*Sympetrum flaveolum*) flight: Kinematic measurement and modelling. *J. Fluids Struct.* **2013**, *40*, 115–126. [CrossRef]
19. Rajabi, H.; Ghoroubi, N.; Stamm, K.; Appel, E.; Gorb, S. Dragonfly wing nodus: A one-way hinge contributing to the asymmetric wing deformation. *Acta Biomater.* **2017**, *60*, 330–338. [CrossRef] [PubMed]
20. Norberg, R.Å. The pterostigma of insect wings an inertial regulator of wing pitch. *J. Comp. Physiol.* **1972**, *81*, 9–22. [CrossRef]
21. Roskam, J.; Lan, C.-T.E. *Airplane Aerodynamics and Performance*; DARcorporation: Lawrence, KS, USA, 1997.
22. Laliberté, J.F.; Kraemer, K.L.; Dawson, J.W.; Miyata, D. Design and manufacturing of biologically inspired micro aerial vehicle wings using rapid prototyping. *Int. J. Micro Air Veh.* **2013**, *5*, 15–38. [CrossRef]
23. Levy, D.-E.; Seifert, A. Parameter study of simplified dragonfly airfoil geometry at Reynolds number of 6000. *J. Theor. Biol.* **2010**, *266*, 691–702. [CrossRef]
24. Packer, S.; Riservato, E.; Aggio, C. *The Status and Distribution of Dragonflies of the Mediterranean Basin*; IUCN: Gland, Switzerland; Malaga, Spain, 2009.
25. Marden, J. Large-scale changes in thermal sensitivity of flight performance during adult maturation in a dragonfly. *J. Exp. Biol.* **1995**, *198*, 2095–2102.

26. Chitsaz, N.; Marian, R.; Chahl, J. Experimental method for 3D reconstruction of Odonata wings (methodology and dataset). *PLoS ONE* **2020**, *15*, e0232193. [CrossRef]
27. Chitsaz, N.; Chahl, J. Current knowledge of corrugated dragonfly wing structures and future measurement methodology. In Proceedings of the AIAC18: 18th Australian International Aerospace Congress (2019): HUMS—11th Defence Science and Technology (DST) International Conference on Health and Usage Monitoring (HUMS 2019): ISSFD—27th International Symposium on Space Flight Dynamics (ISSFD), Melbourne, Australia, 24–28 February 2019; Engineers Australia, Royal Aeronautical Society: Melbourne, Australia, 2019; pp. 412–417.
28. Combes, S.; Daniel, T. Flexural stiffness in insect wings II. Spatial distribution and dynamic wing bending. *J. Exp. Biol.* **2003**, *206*, 2989–2997. [CrossRef] [PubMed]
29. Stavenga, D.; Stowe, S.; Siebke, K.; Zeil, J.; Arikawa, K. Butterfly wing colours: Scale beads make white pierid wings brighter. *Proc. R. Soc. Lond. Ser. B Biol. Sci.* **2004**, *271*, 1577–1584. [CrossRef] [PubMed]
30. Lindsey, E.; Altizer, S. Sex differences in immune defenses and response to parasitism in monarch butterflies. *Evol. Ecol.* **2009**, *23*, 607–620. [CrossRef]
31. Anholt, B.; Marden, J.H.; Jenkins, D. Patterns of mass gain and sexual dimorphism in adult dragonflies (Insecta: Odonata). *Can. J. Zool.* **1991**, *69*, 1156–1163. [CrossRef]
32. Kulfan, B.M. Universal parametric geometry representation method. *J. Aircr.* **2008**, *45*, 142–158. [CrossRef]
33. Raymer, D. *Aircraft Design: A Conceptual Approach*; American Institute of Aeronautics and Astronautics, Inc.: Reston, VA, USA, 2012.
34. Walker, S.M.; Thomas, A.L.; Taylor, G.K. Photogrammetric reconstruction of high-resolution surface topographies and deformable wing kinematics of tethered locusts and free-flying hoverflies. *J. R. Soc. Interface* **2009**, *6*, 351–366. [CrossRef]
35. Chitsaz, N.; Marian, R.; Chahl, J. Bio-inspired flapping-wing micro air vehicles material properties and evolutionary fabrication. In Proceedings of the AIAC18: 18th Australian International Aerospace Congress (2019): HUMS—11th Defence Science and Technology (DST) International Conference on Health and Usage Monitoring (HUMS 2019): ISSFD—27th International Symposium on Space Flight Dynamics (ISSFD), Melbourne, Australia, 24–28 February 2019; Engineers Australia, Royal Aeronautical Society: Melbourne, Australia, 2019; pp. 425–430.
36. Gaurav, S. Investigation of fluid flow and aerodynamic performance of a corrugated dragonfly wing section: A Review. *Int. J. Res. Aeronaut. Mech. Eng.* **2016**, *4*, 1–9.
37. Steffen, C. Fluid-Structure Interaction Analysis of a Dragonfly Wing. Master's Thesis, Nanyang Technological University, Singapore, 2016.
38. Patel, J.K.; Read, C.B. *Handbook of the Normal Distribution*; CRC Press: Boca Raton, FL, USA, 1996.
39. Wilson, K. Dragonfly giants. *Agrion* **2009**, *13*, 29–31.
40. Rice, W.R. Analyzing tables of statistical tests. *Evolution* **1989**, *43*, 223–225. [CrossRef]
41. Wootton, R. The functional morphology of the wings of Odonata. *Adv. Odonatol.* **1991**, *5*, 153–169.
42. Dileo, C.; Deng, X. Design of and experiments on a dragonfly-inspired robot. *Adv. Robot.* **2009**, *23*, 1003–1021. [CrossRef]
43. Naidu, V.; Young, J.; Lai, J. Effect of wing flexibility on dragonfly Hover flight. In Proceedings of the 19th Australasian Fluid Mechanics Conference, Melbourne, Australia, 8–11 December 2014.
44. Verspui, K.; Wasscher, M.T. The damselfly and dragonfly watercolour collection of Edmond de Selys Longchamps: II Calopterygines, Cordulines, Gomphines and Aeschnines. *Int. J. Odonatol.* **2017**, *20*, 79–112. [CrossRef]

© 2020 by the authors. Licensee MDPI, Basel, Switzerland. This article is an open access article distributed under the terms and conditions of the Creative Commons Attribution (CC BY) license (http://creativecommons.org/licenses/by/4.0/).